

TASAR: Transfer-based Attack on Skeletal Action Recognition

Yunfeng Diao¹, Baiqi Wu^{†1}, Ruixuan Zhang¹,
Ajian Liu², Xingxing Wei³, Meng Wang¹, He Wang^{†4}

¹ Hefei University of Technology, Hefei China

² Institute of Automation, Chinese Academy of Sciences, Beijing China

³ Beihang University, Beijing China

⁴ University College London, London UK

Abstract

Skeletal sequences, as well-structured representations of human behaviors, are crucial in Human Activity Recognition (HAR). The transferability of adversarial skeletal sequences enables attacks in real-world HAR scenarios, such as autonomous driving, intelligent surveillance, and human-computer interactions. However, existing Skeleton-based HAR (S-HAR) attacks exhibit weak adversarial transferability and, therefore, cannot be considered true transfer-based S-HAR attacks. More importantly, the reason for this failure remains unclear. In this paper, we study this phenomenon through the lens of loss surface, and find that its sharpness contributes to the poor transferability in S-HAR. Inspired by this observation, we assume and empirically validate that smoothening the rugged loss landscape could potentially improve adversarial transferability in S-HAR. To this end, we propose the first **Transfer-based Attack on Skeletal Action Recognition**, TASAR. TASAR explores the smoothed model posterior without re-training the pre-trained surrogates, which is achieved by a new post-train Dual Bayesian optimization strategy. Furthermore, unlike previous transfer-based attacks that treat each frame independently and overlook temporal coherence within sequences, TASAR incorporates motion dynamics into the Bayesian attack gradient, effectively disrupting the spatial-temporal coherence of S-HARs. To exhaustively evaluate the effectiveness of existing methods and our method, we build the first large-scale robust S-HAR benchmark, comprising 7 S-HAR models, 10 attack methods, 3 S-HAR datasets and 2 defense models. Extensive results demonstrate the superiority of TASAR. Our benchmark enables easy comparisons for future studies, with the code available in the supplementary material.

Introduction

Human Activity Recognition (HAR) has a wide range of application scenarios, such as human-computer interactions, bio-mechanics, and virtual reality (Sun et al. 2022; Guo et al. 2024a). Skeleton sequences has been widely used in HAR (Yan, Xiong, and Lin 2018), because skeleton data is a well-structured data representation of human behaviors and robust to lighting, occlusion, and view angles. Recent research (Wang et al. 2021; Diao et al. 2021) demonstrates that S-HARs are less robust than expected when adversarial

perturbations are added to the testing data, causing skeletal classifiers to produce incorrect outputs. Previous skeleton-based attacks are mainly developed under the white-box setting (Liu, Akhtar, and Mian 2020; Tanaka, Kera, and Kawamoto 2022), where the attacker knows the structure and parameters of a given model, or under the query-based setting (Diao et al. 2021; Kang et al. 2023a), where the adversary can request numerous queries against the target model (Diao et al. 2024a). But both settings are impractical in real-world HAR scenarios, such as autonomous driving (Guo et al. 2024b), intelligent surveillance (Garcia-Cobo and SanMiguel 2023), and human-computer interactions (Wang et al. 2020), in which the white-box information and a large number of queries are not attainable.

In contrast, transfer-based attacks, which craft adversarial examples from surrogate models and then transfer them to target black-box models, present a more realistic threat under the free-query black-box setting. Although adversarial transferability has been widely studied across various tasks (Huang et al. 2023; Dong et al. 2018; Diao et al. 2024b), research on S-HAR remains limited. Recent studies have attempted to apply white-box S-HAR attacks against black-box models via surrogate models (Wang et al. 2021; Liu, Akhtar, and Mian 2020). However, their transferability is low and highly sensitive to the surrogate choice (Wang et al. 2023; Lu et al. 2023). Consequently, existing S-HAR attacks cannot be regarded as transferable. Similarly, previous transfer-based attacks (Dong et al. 2018; Xiong et al. 2022) are successful on image data, but show poor transferability when applied to skeletal motion. Contrary to the common belief that adversarial examples transfer well across different model architectures and parameters (Liu et al. 2016), existing attacks do not exhibit transferability on S-HAR, raising doubt on the usefulness of adversarial transferability in this domain (Lu et al. 2023). More importantly, the reason for this failure remains unclear.

To study this phenomenon, we begin by examining the factors that hinder adversarial transferability in S-HARs. Our preliminary experiments reveal that adversarial transferability is highly sensitive to the chosen surrogates (Tab. 1). This finding motivates us to further explore the differences between surrogate models from the view of loss surface smoothness, as previous research has demonstrated that the smoothness of the loss surface significantly impacts adver-

[†]Corresponding author, 2021214516@mail.hfut.edu.cn,
h.e.wang@leeds.ac.uk

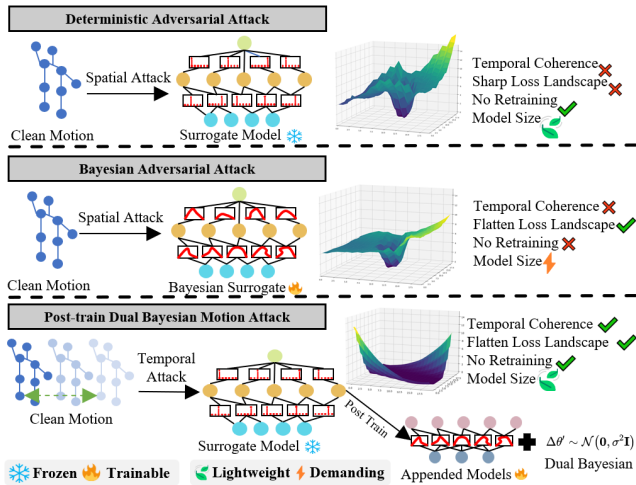


Figure 1: A high-level illustration of our proposed method.

sarial transferability (Wu and Zhu 2020; Qin et al. 2022). As shown in Fig. 2, surrogates with a smoothed loss landscape have higher transferability than surrogates with a sharp loss landscape. Therefore, unlike most existing attacks that focus on the backpropagation process, we argue that the S-HAR attack should prioritize smoothing the surrogate’s landscape in the training process.

Bayesian neural networks have been shown to exhibit lower sharpness and better generalization ability (Blundell et al. 2015; Maddox et al. 2019). Therefore, attacking the entire model distribution is more likely to generalize for S-HARs (Li et al. 2023; Gubri et al. 2022). However, it is not straightforward to design such a transferable Bayesian attack for S-HAR. First, skeletal classifiers contain at least several millions of parameters. Sampling from the posterior distribution for such complex models can be computationally expensive and consume a heavy memory footprint. Second, most prior transferable attacks are specifically designed for static data, e.g. images. However, most S-HAR models learn the spatial-temporal features because skeletal data contains rich motion dynamics. Naive adaptation of the Bayesian attack may ignore the spatial-temporal coherence when issuing attacks. How to consider the motion dynamics in Bayesian attacks has not been explored.

To tackle these challenges, we propose the first Transfer-based Attack specifically designed for Skeletal Action Recognition, TASAR, based on a Post-train Dual Bayesian optimization that significantly smoothens the rugged landscape (see Fig. 2). Our post-train Bayesian strategy freezes the pre-trained surrogate and appends small extra Bayesian components behind it, to turn a single surrogate into a Bayesian one without the need for re-training, thereby speeding up the training process and avoiding a heavy memory footprint. Next, we integrate the temporal motion gradient in a Bayesian manner to disrupt the temporal coherence between sequences over time. A high-level illustration of our method is presented in Fig. 1. Our contributions are summarized as follows.

- We systematically investigate the previously unknown reason for low adversarial transferability in S-HAR through the lens of loss surface smoothness, and introduce the first transfer-based attack on S-HAR to address this issue.
- We propose a novel post-train Dual Bayesian Motion attack, that explores the smoothed model posterior and considers the spatial-temporal coherence from a Bayesian perspective, without requiring re-training of the pre-trained surrogate model.
- We build the first comprehensive robust S-HAR evaluation benchmark *RobustBenchHAR*. *RobustBenchHAR* consists of 7 S-HAR models with diverse GCN structures and more recent Transformer structures, 10 attack methods, 3 datasets and 2 defense methods. Extensive experiments on this benchmark demonstrate the superiority and generalizability of TASAR.

Related Work

Skeleton-Based Human Action Recognition. Early S-HAR research employed convolutional neural networks (CNNs) (Ali et al. 2023) and recurrent neural networks (RNNs) (Du, Wang, and Wang 2015) to extract motion features in the spatial domain and temporal domains, respectively. However, skeleton data, inherently a topological graph, poses challenges for feature representation using traditional CNNs and RNNs. Recent advances with graph convolutional networks (GCNs) (Kipf and Welling 2016) have improved performance by modeling skeletons as topological graphs, with nodes corresponding to joints and edges to bones (Yan, Xiong, and Lin 2018). Subsequent improvements in graph designs and network architectures include two-stream adaptive GCN (2s-AGCN) (Shi et al. 2019b), directed acyclic GCN (DGNN) (Shi et al. 2019a), multi-scale GCN (MS-G3D) (Liu et al. 2020), channel-wise topology refinement (CTR-GCN) (Chen et al. 2021) and auxiliary feature refinement (FR-HEAD) (Zhou, Liu, and Wang 2023). Alongside advancements in GCN-based models, recent studies are exploring temporal Transformer structures for S-HARs (Do and Kim 2024; Qiu et al. 2022; Guo et al. 2024b), but their vulnerability remains unexplored. This work is the first to assess the adversarial robustness of Transformer-based S-HARs.

Adversarial Attacks on S-HAR. Adversarial attacks (Szegedy et al. 2013) highlight the susceptibility of deep neural networks and have been applied across different data types. Recently, attacks on S-HAR have garnered increasing attention. CIASA (Liu, Akhtar, and Mian 2020) proposes a constrained iterative attack via GAN (Goodfellow et al. 2014) to regularize the adversarial skeletons. SMART (Wang et al. 2021) proposes a perception loss gradient. Tanaka et al. (Tanaka, Kera, and Kawamoto 2022) suggest only perturbing skeletal lengths, and evaluate robustness via Fourier analysis (Tanaka, Kera, and Kawamoto 2024). These methods are white-box attacks, requiring full knowledge of the victim model. In contrast, BASAR (Diao et al. 2021, 2024a) proposes motion manifold searching to achieve the query-based black-box

attack. FGDA-GS (Kang et al. 2023b) estimates gradient signs to further reduce query numbers.

Compared to white-box and query-based attacks, transfer-based attacks (Liu et al. 2016) pose a more practical threat as real-world HAR scenarios typically cannot access white-box information or extensive querying. While existing white-box S-HAR attacks (Wang et al. 2021; Liu, Akhtar, and Mian 2020) can be adapted for transfer-based scenarios, they suffer from low transferability and sensitivity to surrogate choices. Lu et al. (Lu et al. 2023) proposes a no-box attack for S-HAR but also lacks transferability. Numerous transfer-based attacks, including gradient-based (Lin et al. 2019), input transformation (Xie et al. 2019), and ensemble-based methods (Xiong et al. 2022; Li et al. 2023), exhibit high transferability across various tasks but struggle in skeletal data (Lu et al. 2023). Therefore, there is an urgent need to develop a transferable attack for skeleton-based action recognition.

Methodology

Preliminaries

We denote a clean motion $\mathbf{x} \in \mathcal{X}$ and its corresponding label $y \in \mathcal{Y}$. Given a surrogate action recognizer f_θ parametrized by θ , f_θ is trained to map a motion \mathbf{x} to a predictive distribution $p(y | \mathbf{x}, \theta)$. The white-box attack can be optimized by minimizing the predictive probability:

$$\arg \min_{\|\tilde{\mathbf{x}} - \mathbf{x}\|_p \leq \epsilon} p(y | \tilde{\mathbf{x}}, \theta) \quad (1)$$

where $\tilde{\mathbf{x}}$ is the adversarial example and ϵ is the perturbation budget. $\|\cdot\|_p$ is the l_p norm distance. The procedure of transfer-based attack is firstly crafting the adversarial example $\tilde{\mathbf{x}}$ by attacking the surrogate model, then transferring $\tilde{\mathbf{x}}$ to attack the unseen target model. In Eq. (1), since the transferable adversarial examples are optimized against one surrogate model, the adversarial transferability heavily relies on the surrogate model learning a classification boundary similar to that of the unknown target model. While possible for image classification, it proves unrealistic for S-HAR (Wang et al. 2023; Lu et al. 2023).

Motivation

Existing S-HAR attacks have shown outstanding white-box attack performance but exhibit low transferability (Wang et al. 2023). Similarly, previous transfer-based attacks (Dong et al. 2018; Xiong et al. 2022), successful on image data, also show poor transferability when applied to skeletal motion (Lu et al. 2023). Naturally, two questions occur to us: (1) *Why do existing adversarial attacks fail to exhibit transferability in skeletal data?* (2) *Do transferable adversarial examples truly exist in S-HAR?*

To answer these questions, we start by generating adversarial examples using various surrogate skeletal recognizers and then evaluate their adversarial transferability. Obviously, in Tab. 1, the transferability is highly sensitive to the chosen surrogates, e.g. CTR-GCN (Chen et al. 2021) as the surrogate exhibits higher transferability than ST-GCN (Yan, Xiong, and Lin 2018). This observation motivates us to further investigate the differences between surrogate models. Previous research (Wu and Zhu 2020; Qin

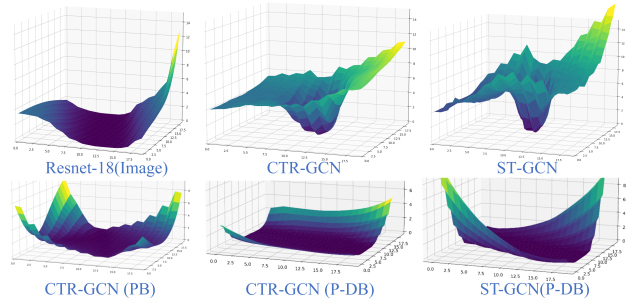


Figure 2: Comparison of loss landscapes of trained models. This visualization method was proposed by (Li et al. 2018), which approximates neural network loss functions in low-dimensional subspaces of the model’s parameter space. The x and y axis represent two random direction vectors. The z axis represents the loss. PB means the post-train Bayesian optimization, and P-DB means the improved post-train Dual Bayesian optimization. The loss landscape optimized by post-train Dual Bayesian is significantly smoother than those of vanilla post-train Bayesian and standard training. More visualizations can be found in Appendix B.

et al. 2022) has proven that adversarial examples generated by surrogate models with a less smooth loss landscape are unlikely to transfer across models. Therefore, we investigate the smoothness of the loss landscape across different surrogate models. In Fig. 2, We visualize the loss landscape of ST-GCN and CTR-GCN trained on the skeletal dataset NTU-60 (Shahroudy et al. 2016) and compare their smoothness to the ResNet-18 (He et al. 2016) trained on CIFAR-10 (Krizhevsky, Hinton et al. 2009). More landscape visualizations can be found in Appendix B. By analyzing the loss surface smoothness, we have two findings: (1) The loss surface of models trained on skeletal data is much sharper than those trained on image data, leading to a relatively low transferability. This suggests that adversarial examples within a sharp local region are less likely to transfer across models in S-HAR, potentially explaining our first question. (2) CTR-GCN has a flatter loss landscape compared to ST-GCN, making it a more effective surrogate for higher transferability. Consequently, we argue that using a surrogate with a smoothed loss landscape will significantly enhance adversarial transferability in S-HAR.

In this work, motivated by evidence that Bayesian neural networks (BNNs) exhibit low sharpness and good generalization (Blundell et al. 2015; Maddox et al. 2019), we aim to construct a Bayesian surrogate by sampling from the model posterior space to smoothen the rugged loss landscape. From a Bayesian perspective, Eq. (1) can be reformulated by approximately minimizing the Bayesian posterior predictive distribution:

$$\arg \min_{\|\tilde{\mathbf{x}} - \mathbf{x}\|_p \leq \epsilon} p(y | \tilde{\mathbf{x}}, \mathcal{D}) = \arg \min_{\|\tilde{\mathbf{x}} - \mathbf{x}\|_p \leq \epsilon} \mathbb{E}_{\theta \sim p(\theta | \mathcal{D})} p(y | \tilde{\mathbf{x}}, \theta) \quad (2)$$

where $p(\theta | \mathcal{D}) \propto p(\mathcal{D} | \theta)p(\theta)$, in which \mathcal{D} is the dataset and $p(\theta)$ is the prior of model weights.

A Post-train Bayesian Perspective on Attack

Unfortunately, directly sampling from the posterior distribution of skeletal classifiers is not a straightforward task due to several factors. First, directly sampling the posterior is intractable for large-scale skeletal classifiers. Although approximate methods such as MCMC sampling (Welling and Teh 2011) or variational inference (Blei, Kucukelbir, and McAuliffe 2017) are possible, sampling is prohibitively slow and resource-intensive due to the high dimensionality of the sampling space, which typically involves at least several million parameters in skeletal classifiers. In addition, skeletal classifiers normally contain a large number of parameters and are pre-trained on large-scale datasets (Liu et al. 2019). Consequently, it is not practical for end-users to re-train the surrogate in a Bayesian manner, as the training process is time-consuming.

To solve the above issues, we propose a new *post-train* Bayesian attack. We maintain the integrity of the pre-trained surrogate while appending a tiny MLP layer $g_{\theta'}$ behind it, connected via a skip connection. Specifically, the final output logits can be computed as: $\text{logits} = g_{\theta'}(f_{\theta}(\mathbf{x})) + f_{\theta}(\mathbf{x})$. In practice, we adopt Monte Carlo sampling to optimize the appended Bayesian model:

$$\begin{aligned} & \max_{\theta'} \mathbb{E}_{\theta' \sim p(\theta' | \mathcal{D}, \theta)} p(y | \mathbf{x}, \theta, \theta') \\ & \approx \max_{\theta'_k} \frac{1}{K} \sum_{k=1}^K p(y | \mathbf{x}, \theta, \theta'_k), \theta'_k \sim p(\theta' | \mathcal{D}, \theta) \end{aligned} \quad (3)$$

where K is the number of appended models. Correspondingly, Eq. (2) can be approximately solved by performing attacks on the ensemble of tiny appended models:

$$\arg \min_{\|\delta\|_p \leq \epsilon} \frac{1}{K} \sum_{k=1}^K p(y | \mathbf{x} + \delta, \theta, \theta'_k), \theta'_k \sim p(\theta' | \mathcal{D}, \theta) \quad (4)$$

Our post-train Bayesian attack offers two advantages. First, the appended models are composed of tiny MLP layers, getting a similar memory cost to a single surrogate. Second, by freezing f_{θ} , our post-train Bayesian strategy keeps the pre-trained surrogate intact, avoiding re-training the pre-trained surrogate. More importantly, training on $g_{\theta'}$ is much faster than on f_{θ} due to the smaller model size of $g_{\theta'}$.

Post-train Dual Bayesian Motion Attack

In our preliminary experiments, we found that a naive application of post-train Bayesian attack (Eq. (4)) already surpassed the adversarial transfer performance of existing S-HAR attacks, which demonstrates the effectiveness of smoothing the loss surface of surrogates. However, its performance remains slightly inferior to the Bayesian attack via re-training a Bayesian surrogate (Li et al. 2023)(Eq. (2)). This performance gap is understandable, as we avoid the prohibitively slow process of sampling the original posterior distribution $\theta \sim p(\theta | \mathcal{D})$ by using a tiny Bayesian component for post-training instead. To further eliminate the trade-off between attack strength and efficiency, we propose a novel post-train dual Bayesian optimization for smoothed posterior sampling, to sample the appended models with

high smoothness for better transferability (Fig. 2). Moreover, unlike previous transfer-based attacks that assume each frame is independent and ignore the temporal dependency between sequences, we integrate motion dynamics information into the Bayesian attack gradient to disrupt the spatial-temporal coherence of S-HAR models. We name our method Post-train Dual Bayesian Motion Attack.

Post-train Dual Bayesian Optimization. This motivation is based on the view that models sampled from a smooth posterior, along with the optimal approximate posterior estimating this smooth posterior, have better smoothness (Nguyen et al. 2024). To this end, we aim for proposing a smooth posterior for learning post-train BNNs, hence possibly possessing higher adversarial transferability. Specifically, inspired by the observation that randomized weights often achieve smoothed weights update (Izmailov et al. 2018; Dziugaite and Roy 2017; Jin et al. 2023), we add Gaussian noise to smooth the appended network weights. This is achieved by a new post-train dual Bayesian optimization:

$$\max_{\theta'} \mathbb{E}_{\theta' \sim p(\theta' | \mathcal{D}, \theta)} \mathbb{E}_{\Delta\theta' \sim \mathcal{N}(\mathbf{0}, \sigma^2 \mathbf{I})} p(y | \mathbf{x}, \theta, \theta' + \Delta\theta') \quad (5)$$

For any appended model sampled from the posterior, Eq. (5) ensures that the neighborhood around the model parameters has uniformly low loss. We further use dual Monte Carlo sampling to approximate Eq. (5):

$$\begin{aligned} & \min_{\theta'_k \sim p(\theta' | \mathcal{D}, \theta)} \frac{1}{MK} \sum_{k=1}^K \sum_{m=1}^M L(\mathbf{x}, y, \theta, \theta'_k + \Delta\theta'_{km}), \\ & \Delta\theta'_{km} \sim \mathcal{N}(\mathbf{0}, \sigma^2 \mathbf{I}) \end{aligned} \quad (6)$$

where L is the classification loss. Considering dual MCMC samplings computationally intensive, we instead consider the worst-case parameters from the posterior, followed by (Li et al. 2023). Hence Eq. (6) can be equivalent to a min-max optimization problem, written as:

$$\begin{aligned} & \min_{\theta'_k \sim p(\theta' | \mathcal{D}, \theta)} \max_{\Delta\theta' \sim \mathcal{N}(\mathbf{0}, \sigma^2 \mathbf{I})} \frac{1}{K} \sum_{k=1}^K L(\mathbf{x}, y, \theta, \theta'_k + \Delta\theta'), \\ & p(\Delta\theta') \geq \xi \end{aligned} \quad (7)$$

The confidence region of the Gaussian posterior is regulated by ξ . We discuss the sensitivity to ξ in the Appendix B. The entanglement between θ' and $\Delta\theta'$ complicates gradient updating. To simplify this issue, we utilize Taylor expansion at θ' to decompose the two components:

$$\begin{aligned} & \min_{\theta'_k \sim p(\theta' | \mathcal{D}, \theta)} \max_{\Delta\theta' \sim \mathcal{N}(\mathbf{0}, \sigma^2 \mathbf{I})} \frac{1}{K} \sum_{k=1}^K [L(\mathbf{x}, y, \theta, \theta'_k) \\ & + \nabla_{\theta'_k} L(\mathbf{x}, y, \theta, \theta'_k)^T \Delta\theta'], p(\Delta\theta') \geq \xi \end{aligned} \quad (8)$$

Since $\Delta\theta'$ is sampled from a zero-mean isotropic Gaussian distribution, the inner maximization can be solved analytically. We introduce the inference details and mathematical deduction in Appendix A. As shown in Fig. 2, the loss landscape optimized by post-train Dual Bayesian is significantly smoother than vanilla post-train Bayesian.

Temporal Motion Gradient in Bayesian Attack. Post-train Dual Bayesian Motion Attack can be performed with gradient-based methods such as FGSM (Goodfellow, Shlens, and Szegedy 2014):

$$\tilde{\mathbf{x}} = \mathbf{x} + \alpha \cdot \text{sign}\left(\sum_{k=1}^K \sum_{m=1}^M \nabla L(\mathbf{x}, y, \theta, \theta'_k + \Delta\theta'_{km})\right) \quad (9)$$

where α is the step size. For notational simplicity, we notate the classification loss $L(\mathbf{x}, y, \theta, \theta'_k + \Delta\theta'_{km})$ as $L(\mathbf{x})$. Assume a motion with t frames $\mathbf{x} = [x_1, x_2, \dots, x_t]$, this attack gradient consists of a set of partial derivatives over all frames $\nabla L(\mathbf{x}) = \left[\frac{\partial L(\mathbf{x})}{\partial x_1}, \frac{\partial L(\mathbf{x})}{\partial x_2}, \dots, \frac{\partial L(\mathbf{x})}{\partial x_t}\right]$. The partial derivative $\frac{\partial L(\mathbf{x})}{\partial x_t}$ assumes each frame is independent, ignoring the dependency between frames over time. This assumption is reasonable for attacks on static data such as PGD (Madry et al. 2017) while infeasible for skeletal motion attacks. In skeletal motion, most S-HAR models learn the spatial-temporal features (Yan, Xiong, and Lin 2018), hence considering motion dynamics in the computing of attack gradient can disrupt the spatial-temporal coherence of these features, leading to more general transferability. To fully represent the motion dynamics, *first-order* (velocity) gradient $(\nabla L(\mathbf{x}))_{d1}$ and *second-order* (acceleration) gradient information $(\nabla L(\mathbf{x}))_{d2}$ should also be considered. To this end, we augment the original *position* gradient with the motion gradient, then Eq. (4) becomes:

$$\tilde{\mathbf{x}} = \mathbf{x} + \alpha \cdot \text{sign}\left(\sum_{k=1}^K \sum_{m=1}^M \nabla L_{dyn}(\mathbf{x})\right) \quad (10)$$

$$\nabla L_{dyn}(\mathbf{x}) = \sum_{n=0}^2 w_n (\nabla L(\mathbf{x}))_{dn}, \quad \sum_{n=0}^2 w_n = 1 \quad (11)$$

where $(\nabla L(\mathbf{x}))_{d0} = \nabla L(\mathbf{x})$. Motion gradient can be computed by explicit modeling (Xia et al. 2015) or implicit learning (Tang et al. 2022). Given that implicit learning requires training an additional data-driven model to learn the motion manifold, which increases computational overhead, we opt for explicit modeling. Inspired by (Lu et al. 2023), we employ time-varying autoregressive models (TV-AR)(Bringmann et al. 2017) because TV-AR can effectively estimate the dynamics of skeleton sequences by modeling the temporary non-stationary signals (Xia et al. 2015). We first use first-order TV-AR(f_{d1}) and second-order TV-AR(f_{d2}) to model human motions respectively:

$$f_{d1} : \tilde{x}_t^i = A_t \cdot \tilde{x}_{t-1}^i + B_t + \gamma_t \quad (12)$$

$$f_{d2} : \tilde{x}_t^i = C_t \cdot \tilde{x}_{t-1}^i + D_t \cdot \tilde{x}_{t-2}^i + E_t + \gamma_t \quad (13)$$

where the model parameters $\beta_t^1 = [A_t, B_t]$ and $\beta_t^2 = [C_t, D_t, E_t]$ are all time-varying parameters and determined by data-fitting. γ_t is a time-dependent white noise representing the dynamics of stochasticity. Using Eq. (12), the first-order motion gradient can be derived as:

$$\left(\frac{\partial L(\tilde{\mathbf{x}}^i)}{\partial \tilde{x}_{t-1}^i}\right)_{d1} = \frac{\partial L(\tilde{\mathbf{x}}^i)}{\partial \tilde{x}_{t-1}^i} + \frac{\partial L(\tilde{\mathbf{x}}^i)}{\partial \tilde{x}_t^i} \cdot A_t \quad (14)$$

Similarly, second-order dynamics can be expressed as below by using Eq. (13):

$$\begin{aligned} \left(\frac{\partial L(\tilde{\mathbf{x}}^i)}{\partial \tilde{x}_{t-2}^i}\right)_{d2} &= \frac{\partial L(\tilde{\mathbf{x}}^i)}{\partial \tilde{x}_{t-2}^i} + \frac{\partial L(\tilde{\mathbf{x}}^i)}{\partial \tilde{x}_{t-1}^i} \cdot C_{t-1} \\ &+ \frac{\partial L(\tilde{\mathbf{x}}^i)}{\partial \tilde{x}_t^i} \cdot (D_t + C_t \cdot C_{t-1}) \end{aligned} \quad (15)$$

where $C_t = \frac{\partial \tilde{x}_t^i}{\partial \tilde{x}_{t-1}^i}$ and $D_t = \frac{\partial \tilde{x}_t^i}{\partial \tilde{x}_{t-2}^i}$. After computing $\tilde{x}_{t-1}^i = C_{t-1} \cdot \tilde{x}_{t-2}^i + D_{t-1} \cdot \tilde{x}_{t-3}^i + E_{t-1} + \gamma_{t-1}$, we can compute $C_{t-1} = \frac{\partial \tilde{x}_{t-1}^i}{\partial \tilde{x}_{t-2}^i}$. Overall, the high-order dynamics gradients over all sequences can be expressed as $(\nabla L(\mathbf{x}))_{d1} = \left[\left(\frac{\partial L(\mathbf{x})}{\partial x_1}\right)_{d1}, \left(\frac{\partial L(\mathbf{x})}{\partial x_2}\right)_{d1}, \dots, \left(\frac{\partial L(\mathbf{x})}{\partial x_t}\right)_{d1}\right]$ and $(\nabla L(\mathbf{x}))_{d2} = \left[\left(\frac{\partial L(\mathbf{x})}{\partial x_1}\right)_{d2}, \left(\frac{\partial L(\mathbf{x})}{\partial x_2}\right)_{d2}, \dots, \left(\frac{\partial L(\mathbf{x})}{\partial x_t}\right)_{d2}\right]$.

Experiments

RobustBenchHAR Settings

To our best knowledge, there is no large-scale benchmark for evaluating transfer-based S-HAR attacks. To fill this gap, we build the first large-scale benchmark for robust S-HAR evaluation, named *RobustBenchHAR*. We briefly introduce the benchmark settings here, with additional details available in Appendix C.

(A) Datasets. *RobustBenchHAR* incorporates three popular S-HAR datasets: NTU 60 (Shahroudy et al. 2016), NTU 120 (Liu et al. 2019) and HDM05(Müller et al. 2007). Since the classifiers do not have the same data pre-processing setting, we unify the data format following (Wang et al. 2023). For NTU 60 and NTU 120, we subsampled frames to 60. For HDM05, we segmented the data into 60-frame samples.

(B) Evaluated Models. We evaluate TASAR in three categories of surrogate/victim models. (1) Normally trained models: We adapt 5 commonly used GCN-based models, i.e., ST-GCN (Yan, Xiong, and Lin 2018), MS-G3D (Liu et al. 2020), CTR-GCN (Chen et al. 2021), 2s-AGCN (Shi et al. 2019b), FR-HEAD (Zhou, Liu, and Wang 2023), and two latest Transformer-based models SkateFormer(Do and Kim 2024) and STTFormer(Qiu et al. 2022). To our best knowledge, this is the first work to investigate the robustness of Transformer-based S-HARs. (2) Ensemble models: an ensemble of ST-CGN, MS-G3D and DGNN (Shi et al. 2019a). (3) Defense models: We employ BEAT (Wang et al. 2023) and TRADES (Zhang et al. 2019), which all demonstrate their robustness for skeletal classifiers.

(C) Baselines. We compare with state-of-the-art (SOTA) S-HAR attacks, i.e. SMART (Wang et al. 2021) and CIASA (Liu, Akhtar, and Mian 2020). We also adopt the SOTA transfer-based attacks as baselines, including gradient-based, i.e., I-FGSM (Kurakin, Goodfellow, and Bengio 2018), MI-FGSM (Dong et al. 2018) and the latest MIG (Ma et al. 2023), input transformation method DIM (Xie et al. 2019), and ensemble-based/Bayesian attacks, i.e., ENS (Dong et al. 2018), SVRE (Xiong et al. 2022) and BA (Li et al. 2023). For a fair comparison, we ran 200 iterations for all attacks under l_∞ norm-bounded perturbation of size 0.01. For TASAR, we use the iterative gradient attack instead of FGSM in Eq. (10).

(D) Implementation Details. Our appended model is a simple two-layer fully-connected layer network. Unless specified otherwise, we use $K = 3$ and $M = 20$ in Eq. (10) for default and explain the reason in the ablation study later. More implementation details can be found in Appendix C.

Evaluation on Normally Trained Models

Evaluation of Untargeted Attack. As shown in in Tab. 1, TASAR significantly surpasses both S-HAR attacks and transfer-based at-

Surrogate	Method	Dataset: NTU60						Ave	Dataset: NTU120						Ave
		Target Models							Target Models						
		ST-GCN	2s-AGCN	MS-G3D	CTR-GCN	FR-HEAD	SFormer	ST-GCN	2s-AGCN	MS-G3D	CTR-GCN	FR-HEAD	SFormer		
ST-GCN	I-FGSM	99.26	11.76	8.33	14.22	16.42	15.44	13.23	96.81	8.82	7.10	13.97	16.42	24.75	14.21
	MI-FGSM	100.00	17.76	27.20	14.95	26.59	11.76	19.65	99.63	18.75	28.18	15.07	20.22	23.03	21.05
	SMART	93.28	5.62	2.19	6.88	7.19	10.08	6.39	94.06	8.28	7.66	11.09	10.16	16.12	10.66
	CIASA	100.00	3.43	3.43	7.60	9.80	8.33	6.52	100.00	4.16	4.41	9.07	8.08	14.95	8.13
	MIG	99.50	25.49	39.60	19.80	36.50	18.14	27.91	98.01	17.45	23.01	15.22	23.76	21.53	20.19
	DIM	77.97	20.54	34.03	12.13	28.83	13.11	21.73	75.61	10.76	12.25	12.75	16.21	23.01	15.00
TASAR	99.29	42.55	64.60	20.33	49.41	17.22	38.82	99.26	19.60	19.37	15.28	22.79	25.24	20.46	
MS-G3D	I-FGSM	25.49	22.79	100.00	20.10	24.75	16.66	21.96	26.96	16.42	100.00	15.20	18.38	27.20	20.83
	MI-FGSM	22.42	13.72	100.00	14.83	20.22	12.25	16.69	25.49	12.25	100.00	14.46	16.78	22.30	18.26
	SMART	21.66	8.96	100.00	12.50	13.54	12.09	13.75	31.25	13.96	100.00	16.04	17.92	23.38	20.51
	CIASA	17.40	5.88	100.00	11.27	11.51	11.76	11.56	22.79	5.88	100.00	11.03	12.50	19.11	14.26
	MIG	31.92	39.65	100.00	24.44	36.15	23.06	31.04	32.17	27.22	100.00	23.27	31.18	33.54	29.48
	DIM	28.58	47.27	100.00	17.82	35.27	17.69	29.33	30.94	38.24	100.00	19.43	30.19	29.82	29.72
TASAR	48.87	51.18	99.61	41.49	40.14	23.90	41.11	41.16	47.28	100.00	28.83	40.60	40.37	39.65	
CTR-GCN	I-FGSM	27.45	16.54	13.72	95.22	44.97	20.71	24.68	33.33	14.95	14.33	97.30	31.00	31.49	25.02
	MI-FGSM	25.36	23.52	36.51	99.02	51.34	19.85	31.32	30.14	19.73	29.16	99.26	29.16	28.30	27.30
	SMART	15.00	5.00	4.69	99.69	15.31	9.27	9.85	19.75	5.84	4.63	99.60	9.27	17.13	11.32
	CIASA	14.70	4.65	5.88	99.75	15.93	9.31	10.09	19.60	5.88	4.65	99.75	10.53	16.91	11.51
	MIG	28.86	35.34	48.19	93.55	53.46	21.04	37.38	30.94	24.75	32.67	94.18	34.03	29.45	30.37
	DIM	23.01	14.97	15.59	53.16	34.71	17.51	21.16	29.51	19.49	24.87	62.31	25.37	23.63	24.57
TASAR	33.76	52.31	66.74	97.06	58.32	21.07	46.44	33.59	26.22	33.82	92.89	35.78	32.84	32.45	
STTFormer	I-FGSM	23.03	15.19	11.27	14.95	16.42	13.48	15.72	26.26	13.97	12.99	15.44	20.83	24.50	19.00
	MI-FGSM	18.13	12.29	19.36	12.25	19.36	10.78	15.36	26.22	21.07	32.35	15.20	22.54	23.77	23.53
	SMART	21.77	6.04	6.04	11.29	10.08	10.88	11.02	23.79	9.27	4.43	9.27	12.90	21.37	13.51
	CIASA	18.62	6.37	5.39	10.54	10.78	10.78	10.41	24.01	10.53	6.61	11.03	15.19	22.30	14.95
	MIG	22.31	21.44	18.89	16.77	23.44	16.77	19.94	30.54	20.32	21.88	16.46	21.25	24.87	22.55
	DIM	23.39	33.04	32.67	15.47	28.71	14.72	24.67	29.82	15.84	14.72	13.99	19.05	24.50	19.65
TASAR	26.44	54.32	42.78	16.35	37.98	18.38	32.71	34.61	34.61	46.63	19.71	32.21	26.92	32.45	

Table 1: The attack success rate(%) of untargeted transfer-based attacks on NTU60 and NTU120. ‘Ave’ was calculated as the average transfer success rate over all target models except for the surrogate. ‘SFormer’ means SkateFormer.

tacks under the black-box settings, while maintaining comparable white-box attack performance. Specially, TASAR achieves the highest average transfer success rate of **35.5%** across different models and datasets, surpassing SMART (Wang et al. 2021) (the SOTA S-HAR attack) and MIG (Ma et al. 2023) (the SOTA transfer-based attack) by a large margin of **23.4%** and **8.1%** respectively. Moreover, TASAR shows consistent transferability across all surrogate models, target models and datasets. These improvements break the common belief that transfer-based attacks in S-HAR suffer from low transferability and highly rely on the chosen surrogate (Lu et al. 2023).

Evaluation of Targeted Attack. In this section, we focus on targeted attacks under the black-box setting. Improving targeted attack transferability on S-HAR is generally more challenging than untargeted attacks. This is primarily due to the significant semantic differences between the randomly selected class and the original one. Attacking a ‘running’ motion to ‘walking’ is generally easier than to ‘drinking’. This is why targeted attacks have lower success rate than untargeted attacks. However, Tab. 2 shows TASAR still outperforms the baseline under most scenarios. Moreover, TASAR can successfully attack the original class to a target with an obvious semantic gap without being detected by humans. The visual examples can be found in Appendix B.

Evaluation on Ensemble and Defense Models

Evaluation on Ensemble Models. TASAR benefits from the additional model parameters added by the appended Bayesian components. For a fair comparison, we compare it with SOTA ensemble-based methods, i.e., ENS (Dong et al. 2018) and SVRE (Xiong et al. 2022), and the Bayesian Attack (BA) (Li et al. 2023), because they also benefit from the model size. Unlike BA, which re-trains the surrogate into a BNN, we instead append a small Bayesian component for post-training. ENS and SVRE take three models ST-GCN, MS-G3D and DGNN as an ensemble of surrogate models, while BA and TASAR only take MS-G3D as the single substi-

Surrogate	Method	Target					Ave
		ST-GCN	2s-AGCN	MS-G3D	CTR-GCN	FR-HEAD	
ST-GCN	MI-FGSM	27.45	3.06	2.32	1.71	1.71	2.20
	SMART	28.02	1.20	1.81	1.41	1.81	1.56
	TASAR	28.79	6.06	6.06	8.33	6.82	6.82
MS-G3D	MI-FGSM	2.08	3.31	32.72	1.83	2.45	2.42
	SMART	0.80	0.60	44.95	1.01	1.01	0.86
	TASAR	9.09	9.09	57.58	9.85	9.33	9.34
CTR-GCN	MI-FGSM	3.06	3.30	2.81	29.53	4.53	3.43
	SMART	1.61	1.61	1.61	43.95	1.81	1.66
	TASAR	8.33	9.09	8.33	22.73	9.09	8.71
2s-AGCN	MI-FGSM	1.47	98.61	1.83	1.83	1.47	1.65
	SMART	2.21	53.02	1.20	2.62	2.21	2.06
	TASAR	10.61	76.52	4.56	10.61	8.33	8.53

Table 2: The targeted attack success rate (%) of targeted transfer-based attack on NTU60.

tute architecture. We choose ST-GCN, 2s-AGCN, MS-G3D, CTR-GCN, FR-HEAD as the target models, and evaluate the average white-box attack success rate (WASR), average black-box attack success (BASR) and the number of parameters in Fig. 3. We can clearly see that TASAR (blue line) achieves the best attack performance under both white-box and black-box settings, with an order of magnitude smaller model size. When using MSG3D (12.78M) as the surrogate model, the Bayesian components appended by TASAR only increase 0.012M parameters of the surrogate size, resulting in a memory cost comparable to that of a single surrogate. In contrast, the Bayesian surrogate model used by BA has 15 times more parameters (255.57M) than the single surrogate.

Evaluation on Defense Models. As BEAT shows high robustness against S-HAR white-box attack (Wang et al. 2023), it is also interesting to evaluate its defense performance against black-box attack. We also employ the adversarial training method TRADES (Zhang et al. 2019) as a baseline due to its robustness in S-HAR (Wang et al. 2023). Obviously, in Tab. 3, TASAR still achieves the highest adversarial transferability among the compared methods against defense models, further validating its effectiveness.

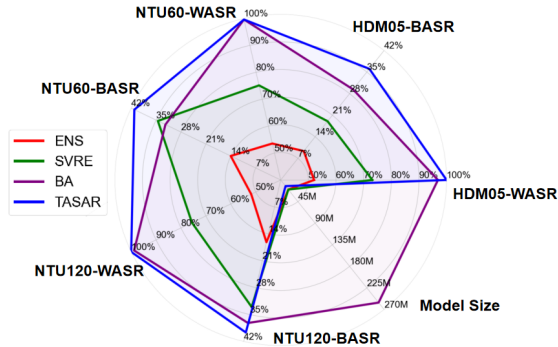


Figure 3: Comparisons with ensemble and Bayesian attacks. We calculate the model size and evaluate the average white-box (WASR) and black-box attack success rate (BASR) on the HDM05, NTU60, and NTU120 datasets, respectively.

Surrogate	Method	TRADES			BEAT		
		ST-GCN	MS-G3D	CTR-GCN	STGCN	MS-G3D	CTR-GCN
ST-GCN	MI-FGSM	3.95	3.75	3.54	96.45	22.29	16.45
	SMART	2.81	3.13	1.88	80.13	3.34	2.90
	TASAR(Ours)	3.92	4.17	2.94	92.19	60.16	39.84
MS-G3D	MI-FGSM	3.02	3.02	2.42	36.89	100.00	30.64
	SMART	2.50	3.13	3.13	6.69	82.36	4.01
	TASAR(Ours)	12.26	10.29	12.25	59.38	100.00	58.59
ST-GCN	MI-FGSM	16.05	5.51	8.46	95.83	30.39	16.05
	SMART	12.50	5.78	9.06	73.95	4.68	8.28
	TASAR(Ours)	12.50	10.22	12.50	97.98	52.34	19.53
MS-G3D	MI-FGSM	23.4	7.59	13.11	28.06	97.54	16.54
	SMART	19.45	7.42	11.72	26.71	79.68	13.82
	TASAR(Ours)	19.79	14.58	17.71	40.63	100.00	32.29

Table 3: The untarget attack success rate (%) against defense models on HDM05 (top) and NTU 60 (bottom). The surrogate models are normally trained without robustness to adversarial examples, whereas the target models are trained using defense methods.

Ablation Study

Dual MCMC Sampling. TASAR proposes a new dual MCMC sampling in the post-train Bayesian formulation (Eq. (10)). To see its contribution, we conduct an ablation study on the number of appended models (K and M in Eq. (10)). As shown in Tab. 4, compared with vanilla Post-train Bayesian strategy ($M=0$), the dual sampling significantly improves the attack performance. Furthermore, although TASAR theoretically requires intensive sampling for inference, in practice, we find a small number of sampling is sufficient ($K = 3$ and $M = 20$). More sampling will cause extra computation overhead. So we use $K = 3$ and $M = 20$ by default.

Temporal Motion Gradient. TASAR benefits from the interplay between temporal Motion Gradient (MG) and Bayesian manner. We hence conduct ablation studies (MG/No MG) to show the effects of motion gradient and report the results in Tab. 5. Compared with TASAR without using motion gradient, TASAR with motion gradient consistently improves the attack success rate in both white box and transfer-based attacks, which shows the benefit of integrating the motion gradient into the Bayesian formulation.

Surrogate Transferability

It is widely believed that transfer-based attacks in S-HAR are highly sensitive to the surrogate choice (Lu et al. 2023; Wang et al. 2023, 2021). In this subsection, we provide a detailed analysis of the factors contributing to this phenomenon. When looking at the results in Tab. 1 and the visualization of loss landscape in Fig. 2 and Appendix B, we note that loss surface smoothness correlates

K	M	Target				
		ST-GCN	2s-AGCN	MS-G3D	CTR-GCN	FR-HEAD
1	0	97.46	39.06	58.39	19.53	43.75
	10	98.24	40.23	60.35	19.14	45.31
	20	98.05	41.21	59.57	18.36	45.72
3	0	97.46	39.25	56.45	19.34	43.16
	10	98.07	42.01	60.57	19.73	46.49
	20	99.29	42.55	64.60	20.33	49.41
5	0	97.92	36.21	56.77	18.75	41.92
	10	96.88	41.15	63.80	16.93	45.05
	20	97.14	39.84	60.94	20.57	45.21

Table 4: Ablation Study on NTU 60 with ST-GCN as the surrogate. M and K are the number dual MCMC sampling in Eq. (10). To isolate the impact of the number of appended models, we employ TASAR without motion gradient. The contribution of the motion gradient will be discussed in the subsequent ablation experiment.

Dataset	Surrogate	Motion	Target				
			ST-GCN	2s-AGCN	MS-G3D	CTR-GCN	FR-HEAD
HDM05	ST-GCN	No MG	96.81	13.23	58.58	38.97	17.89
		MG	97.30	14.26	60.54	37.50	23.43
		MS-G3D	No MG	46.28	38.74	97.79	36.27
NTU60	ST-GCN	No MG	98.77	33.74	54.97	17.87	37.50
		MG	99.29	42.45	64.60	20.33	46.07
		MS-G3D	No MG	40.60	48.69	99.61	37.51
NTU120	ST-GCN	No MG	98.53	20.83	24.46	14.71	21.81
		MG	99.26	19.60	19.37	15.28	22.79
		MS-G3D	No MG	34.64	36.27	100.00	25.49
		MG	41.16	47.28	100.00	28.83	40.60

Table 5: The ablation experiments of motion gradient. ‘MG’ means TASAR with motion gradient, ‘No MG’ means TASAR without using motion gradient.

with the adversarial transferability. For example, CTR-GCN, manifesting smoother regions within the loss landscape, demonstrates higher transferability than ST-GCN and STTFormer. STTFormer trained on NTU 120 has a smoother loss surface than ST-GCN (see Appendix B), resulting in higher transferability than ST-GCN. For NTU 60, STTFormer shows a similar loss surface to that of ST-GCN and exhibits comparable transferability. Therefore, we suspect that the loss surface smoothness plays a pivotal role in boosting adversarial transferability for S-HAR, potentially outweighing the significance of gradient-based optimization techniques. Next, two-stream MS-G3D shows the highest transferability. Unlike other surrogates, which solely extract joint information, MS-G3D uses a two-stream ensemble incorporating both joint and bone features, thereby effectively capturing relative joint movements. In conclusion, we suggest that skeletal transfer-based attacks employ smoother two-stream surrogates incorporating both joint and bone information.

Conclusion

In this paper, we systematically investigate the adversarial transferability for S-HARs from the view of loss landscape, and propose the first transfer-based attack on skeletal action recognition, TASAR. We build *RobustBenchHAR*, the first comprehensive benchmark for robustness evaluation in S-HAR. We hope that *RobustBenchHAR* could contribute to the adversarial learning and S-HAR community by facilitating researchers to easily compare new methods with existing ones and inspiring new research from the thorough analysis of the comprehensive evaluations.

References

- Ali, A.; Pinyoanunpong, E.; Wang, P.; and Dorodchi, M. 2023. Skeleton-based Human Action Recognition via Convolutional Neural Networks (CNN). *arXiv preprint arXiv:2301.13360*.
- Blei, D. M.; Kucukelbir, A.; and McAuliffe, J. D. 2017. Variational inference: A review for statisticians. *Journal of the American statistical Association*, 112(518): 859–877.
- Blundell, C.; Cornebise, J.; Kavukcuoglu, K.; and Wierstra, D. 2015. Weight uncertainty in neural network. In *International conference on machine learning*, 1613–1622. PMLR.
- Bringmann, L. F.; Hamaker, E. L.; Vigo, D. E.; Aubert, A.; Borsboom, D.; and Tuerlinckx, F. 2017. Changing dynamics: Time-varying autoregressive models using generalized additive modeling. *Psychological methods*, 22(3): 409.
- Chen, Y.; Zhang, Z.; Yuan, C.; Li, B.; Deng, Y.; and Hu, W. 2021. Channel-wise topology refinement graph convolution for skeleton-based action recognition. In *Proceedings of the IEEE/CVF international conference on computer vision*, 13359–13368.
- Diao, Y.; Shao, T.; Yang, Y.-L.; Zhou, K.; and Wang, H. 2021. BASAR: Black-Box Attack on Skeletal Action Recognition. In *Proceedings of the IEEE/CVF Conference on Computer Vision and Pattern Recognition (CVPR)*, 7597–7607.
- Diao, Y.; Wang, H.; Shao, T.; Yang, Y.; Zhou, K.; Hogg, D.; and Wang, M. 2024a. Understanding the vulnerability of skeleton-based Human Activity Recognition via black-box attack. *Pattern Recognition*, 153: 110564.
- Diao, Y.; Zhai, N.; Miao, C.; Yang, X.; and Wang, M. 2024b. Vulnerabilities in AI-generated Image Detection: The Challenge of Adversarial Attacks. *arXiv preprint arXiv:2407.20836*.
- Do, J.; and Kim, M. 2024. SkateFormer: Skeletal-Temporal Transformer for Human Action Recognition. In *European Conference on Computer Vision (ECCV)*.
- Dong, Y.; Liao, F.; Pang, T.; Su, H.; Zhu, J.; Hu, X.; and Li, J. 2018. Boosting Adversarial Attacks With Momentum. In *Proceedings of the IEEE Conference on Computer Vision and Pattern Recognition (CVPR)*.
- Du, Y.; Wang, W.; and Wang, L. 2015. Hierarchical recurrent neural network for skeleton based action recognition. In *Proceedings of the IEEE conference on computer vision and pattern recognition*, 1110–1118.
- Dziugaite, G. K.; and Roy, D. M. 2017. Computing Nonvacuous Generalization Bounds for Deep (Stochastic) Neural Networks with Many More Parameters than Training Data. In *Proceedings of the Thirty-Third Conference on Uncertainty in Artificial Intelligence, UAI*.
- Garcia-Cobo, G.; and SanMiguel, J. C. 2023. Human skeletons and change detection for efficient violence detection in surveillance videos. *Computer Vision and Image Understanding*, 233: 103739.
- Goodfellow, I.; Pouget-Abadie, J.; Mirza, M.; Xu, B.; Warde-Farley, D.; Ozair, S.; Courville, A.; and Bengio, Y. 2014. Generative adversarial nets. *Advances in neural information processing systems*, 27.
- Goodfellow, I. J.; Shlens, J.; and Szegedy, C. 2014. Explaining and harnessing adversarial examples. *arXiv preprint arXiv:1412.6572*.
- Gubri, M.; Cordy, M.; Papadakis, M.; Le Traon, Y.; and Sen, K. 2022. Efficient and transferable adversarial examples from bayesian neural networks. In *Uncertainty in Artificial Intelligence*, 738–748. PMLR.
- Guo, D.; Li, K.; Hu, B.; Zhang, Y.; and Wang, M. 2024a. Benchmarking Micro-action Recognition: Dataset, Method, and Application. *IEEE Transactions on Circuits and Systems for Video Technology*.
- Guo, X.; Zhu, Q.; Wang, Y.; and Mo, Y. 2024b. MG-GCT: A Motion-Guided Graph Convolutional Transformer for Traffic Gesture Recognition. *IEEE Transactions on Intelligent Transportation Systems*.
- He, K.; Zhang, X.; Ren, S.; and Sun, J. 2016. Deep residual learning for image recognition. In *Proceedings of the IEEE conference on computer vision and pattern recognition*, 770–778.
- Huang, H.; Chen, Z.; Chen, H.; Wang, Y.; and Zhang, K. 2023. T-SEA: Transfer-Based Self-Ensemble Attack on Object Detection. In *Proceedings of the IEEE/CVF Conference on Computer Vision and Pattern Recognition (CVPR)*, 20514–20523.
- Izmailov, P.; Podoprikin, D.; Garipov, T.; Vetrov, D.; and Wilson, A. G. 2018. Averaging weights leads to wider optima and better generalization. In *34th Conference on Uncertainty in Artificial Intelligence 2018, UAI 2018*, 876–885.
- Jin, G.; Yi, X.; Wu, D.; Mu, R.; and Huang, X. 2023. Randomized adversarial training via taylor expansion. In *Proceedings of the IEEE/CVF Conference on Computer Vision and Pattern Recognition*, 16447–16457.
- Kang, Z.; Xia, H.; Zhang, R.; Jiang, S.; Shi, X.; and Zhang, Z. 2023a. FGDA-GS: Fast guided decision attack based on gradient signs for skeletal action recognition. *Computers & Security*, 135: 103522.
- Kang, Z.; Xia, H.; Zhang, R.; Jiang, S.; Shi, X.; and Zhang, Z. 2023b. FGDA-GS: Fast guided decision attack based on gradient signs for skeletal action recognition. *Computers & Security*, 135: 103522.
- Kipf, T. N.; and Welling, M. 2016. Semi-Supervised Classification with Graph Convolutional Networks. *CoRR*, abs/1609.02907.
- Krizhevsky, A.; Hinton, G.; et al. 2009. Learning multiple layers of features from tiny images.
- Kurakin, A.; Goodfellow, I. J.; and Bengio, S. 2018. Adversarial examples in the physical world. In *Artificial intelligence safety and security*, 99–112. Chapman and Hall/CRC.
- Li, H.; Xu, Z.; Taylor, G.; Studer, C.; and Goldstein, T. 2018. Visualizing the loss landscape of neural nets. *Advances in neural information processing systems*, 31.
- Li, Q.; Guo, Y.; Zuo, W.; and Chen, H. 2023. Making Substitute Models More Bayesian Can Enhance Transferability of Adversarial Examples. In *The Eleventh International Conference on Learning Representations, ICLR 2023, Kigali, Rwanda, May 1-5, 2023*.
- Lin, J.; Song, C.; He, K.; Wang, L.; and Hopcroft, J. E. 2019. Nesterov accelerated gradient and scale invariance for adversarial attacks. *arXiv preprint arXiv:1908.06281*.
- Liu, J.; Akhtar, N.; and Mian, A. 2020. Adversarial attack on skeleton-based human action recognition. *IEEE Transactions on Neural Networks and Learning Systems*, 33(4): 1609–1622.
- Liu, J.; Shahroudy, A.; Perez, M.; Wang, G.; Duan, L.-Y.; and Kot, A. C. 2019. Ntu rgb+ d 120: A large-scale benchmark for 3d human activity understanding. *IEEE transactions on pattern analysis and machine intelligence*, 42(10): 2684–2701.
- Liu, Y.; Chen, X.; Liu, C.; and Song, D. 2016. Delving into Transferable Adversarial Examples and Black-box Attacks. In *International Conference on Learning Representations*.
- Liu, Z.; Zhang, H.; Chen, Z.; Wang, Z.; and Ouyang, W. 2020. Disentangling and unifying graph convolutions for skeleton-based action recognition. In *Proceedings of the IEEE/CVF conference on computer vision and pattern recognition*, 143–152.

- Lu, Z.; Wang, H.; Chang, Z.; Yang, G.; and Shum, H. P. H. 2023. Hard No-Box Adversarial Attack on Skeleton-Based Human Action Recognition with Skeleton-Motion-Informed Gradient. In *Proceedings of the IEEE/CVF International Conference on Computer Vision (ICCV)*, 4597–4606.
- Ma, W.; Li, Y.; Jia, X.; and Xu, W. 2023. Transferable adversarial attack for both vision transformers and convolutional networks via momentum integrated gradients. In *Proceedings of the IEEE/CVF International Conference on Computer Vision*, 4630–4639.
- Maddox, W. J.; Izmailov, P.; Garipov, T.; Vetrov, D. P.; and Wilson, A. G. 2019. A simple baseline for bayesian uncertainty in deep learning. *Advances in neural information processing systems*, 32.
- Madry, A.; Makelov, A.; Schmidt, L.; Tsipras, D.; and Vladu, A. 2017. Towards deep learning models resistant to adversarial attacks. *arXiv preprint arXiv:1706.06083*.
- Müller, M.; Röder, T.; Clausen, M.; Eberhardt, B.; Krüger, B.; and Weber, A. 2007. Mocap database hdm05. *Institut für Informatik II, Universität Bonn*, 2(7).
- Nguyen, V.-A.; Vuong, T.-L.; Phan, H.; Do, T.-T.; Phung, D.; and Le, T. 2024. Flat seeking bayesian neural networks. *Advances in Neural Information Processing Systems*, 36.
- Qin, Z.; Fan, Y.; Liu, Y.; Shen, L.; Zhang, Y.; Wang, J.; and Wu, B. 2022. Boosting the transferability of adversarial attacks with reverse adversarial perturbation. *Advances in Neural Information Processing Systems*, 35: 29845–29858.
- Qiu, H.; Hou, B.; Ren, B.; and Zhang, X. 2022. Spatio-Temporal Tuples Transformer for Skeleton-Based Action Recognition. *CoRR*, abs/2201.02849.
- Shahroudy, A.; Liu, J.; Ng, T.-T.; and Wang, G. 2016. Ntu rgb+ d: A large scale dataset for 3d human activity analysis. In *Proceedings of the IEEE conference on computer vision and pattern recognition*, 1010–1019.
- Shi, L.; Zhang, Y.; Cheng, J.; and Lu, H. 2019a. Skeleton-based action recognition with directed graph neural networks. In *Proceedings of the IEEE/CVF conference on computer vision and pattern recognition*, 7912–7921.
- Shi, L.; Zhang, Y.; Cheng, J.; and Lu, H. 2019b. Two-stream adaptive graph convolutional networks for skeleton-based action recognition. In *Proceedings of the IEEE/CVF conference on computer vision and pattern recognition*, 12026–12035.
- Sun, Z.; Ke, Q.; Rahmani, H.; Bennamoun, M.; Wang, G.; and Liu, J. 2022. Human action recognition from various data modalities: A review. *IEEE transactions on pattern analysis and machine intelligence*, 45(3): 3200–3225.
- Szegedy, C.; Zaremba, W.; Sutskever, I.; Bruna, J.; Erhan, D.; Goodfellow, I.; and Fergus, R. 2013. Intriguing properties of neural networks. *arXiv preprint arXiv:1312.6199*.
- Tanaka, N.; Kera, H.; and Kawamoto, K. 2022. Adversarial bone length attack on action recognition. In *Proceedings of the AAAI Conference on Artificial Intelligence*, volume 36, 2335–2343.
- Tanaka, N.; Kera, H.; and Kawamoto, K. 2024. Fourier analysis on robustness of graph convolutional neural networks for skeleton-based action recognition. *Computer Vision and Image Understanding*, 240: 103936.
- Tang, X.; Wang, H.; Hu, B.; Gong, X.; Yi, R.; Kou, Q.; and Jin, X. 2022. Real-time controllable motion transition for characters. *ACM Transactions on Graphics (TOG)*, 41(4): 1–10.
- Wang, H.; Diao, Y.; Tan, Z.; and Guo, G. 2023. Defending Black-Box Skeleton-Based Human Activity Classifiers. In Williams, B.; Chen, Y.; and Neville, J., eds., *Thirty-Seventh AAAI Conference on Artificial Intelligence*, 2546–2554.
- Wang, H.; He, F.; Peng, Z.; Shao, T.; Yang, Y.-L.; Zhou, K.; and Hogg, D. 2021. Understanding the robustness of skeleton-based action recognition under adversarial attack. In *Proceedings of the IEEE/CVF Conference on Computer Vision and Pattern Recognition*, 14656–14665.
- Wang, T.; Yang, T.; Danelljan, M.; Khan, F. S.; Zhang, X.; and Sun, J. 2020. Learning human-object interaction detection using interaction points. In *Proceedings of the IEEE/CVF Conference on Computer Vision and Pattern Recognition*, 4116–4125.
- Welling, M.; and Teh, Y. W. 2011. Bayesian learning via stochastic gradient Langevin dynamics. In *Proceedings of the 28th international conference on machine learning (ICML-11)*, 681–688. Cite-seer.
- Wu, L.; and Zhu, Z. 2020. Towards understanding and improving the transferability of adversarial examples in deep neural networks. In *Asian Conference on Machine Learning*, 837–850. PMLR.
- Xia, S.; Wang, C.; Chai, J.; and Hodgins, J. 2015. Realtime style transfer for unlabeled heterogeneous human motion. *ACM Transactions on Graphics (TOG)*, 34(4): 1–10.
- Xie, C.; Zhang, Z.; Zhou, Y.; Bai, S.; Wang, J.; Ren, Z.; and Yuille, A. L. 2019. Improving transferability of adversarial examples with input diversity. In *Proceedings of the IEEE/CVF conference on computer vision and pattern recognition*, 2730–2739.
- Xiong, Y.; Lin, J.; Zhang, M.; Hopcroft, J. E.; and He, K. 2022. Stochastic variance reduced ensemble adversarial attack for boosting the adversarial transferability. In *Proceedings of the IEEE/CVF Conference on Computer Vision and Pattern Recognition*, 14983–14992.
- Yan, S.; Xiong, Y.; and Lin, D. 2018. Spatial temporal graph convolutional networks for skeleton-based action recognition. In *Proceedings of the AAAI conference on artificial intelligence*, volume 32.
- Zhang, H.; Yu, Y.; Jiao, J.; Xing, E.; El Ghaoui, L.; and Jordan, M. 2019. Theoretically principled trade-off between robustness and accuracy. In *International conference on machine learning*, 7472–7482. PMLR.
- Zhou, H.; Liu, Q.; and Wang, Y. 2023. Learning Discriminative Representations for Skeleton Based Action Recognition. In *Proceedings of the IEEE/CVF Conference on Computer Vision and Pattern Recognition (CVPR)*, 10608–10617.

Reproducibility Checklist

This paper:

- Includes a conceptual outline and/or pseudocode description of AI methods introduced (**yes**)
- Clearly delineates statements that are opinions, hypothesis, and speculation from objective facts and results (**yes**)
- Provides well marked pedagogical references for less-familiar readers to gain background necessary to replicate the paper (**yes**)

Does this paper make theoretical contributions? (**no**)

Does this paper rely on one or more datasets? (yes) If yes, please complete the list below.

- A motivation is given for why the experiments are conducted on the selected datasets (**yes**)
- All novel datasets introduced in this paper are included in a data appendix. (NA)
- All novel datasets introduced in this paper will be made publicly available upon publication of the paper with a license that allows free usage for research purposes. (NA)
- All datasets drawn from the existing literature (potentially including authors' own previously published work) are accompanied by appropriate citations. (**yes**)
- All datasets drawn from the existing literature (potentially including authors' own previously published work) are publicly available. (**yes**)
- All datasets that are not publicly available are described in detail, with explanation why publicly available alternatives are not scientifically satisfying. (NA)

Does this paper include computational experiments? (yes) If yes, please complete the list below.

- Any code required for pre-processing data is included in the appendix. (**yes**).
- All source code required for conducting and analyzing the experiments is included in a code appendix. (**yes**)
- All source code required for conducting and analyzing the experiments will be made publicly available upon publication of the paper with a license that allows free usage for research purposes. (**yes**)
- All source code implementing new methods have comments detailing the implementation, with references to the paper where each step comes from (**yes**)
- If an algorithm depends on randomness, then the method used for setting seeds is described in a way sufficient to allow replication of results. (**yes**)
- This paper specifies the computing infrastructure used for running experiments (hardware and software), including GPU/CPU models; amount of memory; operating system; names and versions of relevant software libraries and frameworks. (**yes**)
- This paper formally describes evaluation metrics used and explains the motivation for choosing these metrics. (**yes**)
- This paper states the number of algorithm runs used to compute each reported result. (**yes**)
- Analysis of experiments goes beyond single-dimensional summaries of performance (e.g., average; median) to include measures of variation, confidence, or other distributional information. (**yes**)

- The significance of any improvement or decrease in performance is judged using appropriate statistical tests (e.g., Wilcoxon signed-rank). (**yes**)
- This paper lists all final (hyper-)parameters used for each model/algorithm in the paper's experiments. (**yes**)
- This paper states the number and range of values tried per (hyper-) parameter during development of the paper, along with the criterion used for selecting the final parameter setting. (**yes**)